J. Fluid Mech. (1997), *vol.* 337, *pp.* 381–410

The effects of surfactant on the dynamics of bubble snap-off

By T. M. TSAI AND MICHAEL J. MIKSIS

Department of Engineering Sciences and Applied Mathematics, Northwestern University, Evanston, IL 60208, USA

(Received 5 June 1995 and in revised form 25 November 1996)

The effects of an insoluble surfactant on the motion of a drop or bubble as it is driven by a pressure gradient through a capillary tube is investigated numerically. We find that a drop in a straight capillary tube can either approach a steady-state shape or develop a re-entrant cavity at its rear. For a gas bubble moving through a constricted capillary tube, we find that snap-off can occur and surfactants enhance the snap-off process. The effects of the parameters on the dynamics of bubble snap-off are illustrated and discussed.

1. Introduction

Surface-active impurities are encountered in many industrial applications of multi-phase flows. In some situations they are added to the process to improve the result, while in other situations their presence is not positive but they are difficult to remove from the system. Hence it is important to understand the effects of surfactant on the dynamics of multi-phase flows. Here we will study the effects of an insoluble surfactant on the dynamics of a bubble or drop in a constricted capillary tube. In particular, we are interested in examining the effects of the surfactant on the snap-off process (Roof 1970) which occurs as a bubble or drop passes through a constriction.

Since interfacial tension forces are very sensitive to the presence of minute amounts of surface-active impurities, their presence can lead to a significant variation of these forces along a fluid–fluid interface. The resulting interfacial tension gradients lead to tangential (Marangoni) stresses which affect the motion of the fluid–fluid interface. One example of the use of surfactant is in enhanced oil recovery where they are used as an aid in the formation of foams in porous media. The surfactant will affect the size of the bubbles being generated in the foam and the stability of a lamella after the generation of the foam. Another example is motivated by an interest in the interaction between inhaled droplets and the lung's thin liquid lining after an aerosol lands on its surface, e.g. see Grotberg (1994) for a review of this subject.

There has been a considerable number of studies on the transport of bubbles and drops in capillary tubes without surfactant, e.g. see Olbricht (1996) for a review of this subject. Fewer studies have been done with the presence of surfactant because of the increased difficulty of the problem. For the steady translation of a drop in straight capillary tube, Borhan & Mao (1992) computed the steady solutions of a drop translating in a straight capillary tube including the effects of an insoluble surfactant. In a frame of reference moving with the steady velocity of the drop, they found that the Marangoni stresses oppose surface convection and retard the motion of the drop as a whole. Assuming that the drop remains spherical, He, Dagan & Maldarelli (1991)

studied the influence of surfactant adsorption on the motion of a drop and confirmed the retarding effect of surfactant on a neutrally buoyant drop. The influence of soluble surfactant on the steady translation of a finite or semi-infinite bubble in a straight capillary was investigated by Ginley & Radke (1989), Ratulowski & Chang (1990) and Park (1992). One of the aims of these works was to estimate the influence of surfactant on the film thickness between the bubble surface and the tube wall. Ginley & Radke (1989) assumed that the surfactant concentration in the suspending fluid was uniform and adsorption was the rate-controlling mechanism of the surfactant transport. They found that the film thickness between the bubble surface and the tube wall decreases compared to the surfactant-free case. Ratulowski & Chang (1990) showed that the film thickness can increase by a maximum factor of $4^{2/3}$ compared to the surfactant-free case if the surfactant transport in the thin film is limited by the mass transfer from the suspending fluid ahead of the bubble. Park (1992) analysed the motion of a finite bubble, and found that film thickening occurs due to the accumulation of the surfactant at the trailing end of the bubble only when the bubble length is larger than a certain critical value. Wassmuth, Laidlaw & Coombe (1993) studied the effects of soluble surfactant on the two-dimensional motion of a semi-infinite bubble moving between two parallel plates with and without a constriction. Using a finite difference method, they solved the Navier–Stokes equations and the convection–diffusion equation for the surfactant transport in the bulk fluid. However, as these authors have noted, the two-dimensional parallel plate system lacks the additional effects of surface minimization which occurs in a cylindrical setting. Namely, when a drop or bubble is moving through a constriction, its radius at the constriction is decreasing, and this can be accounted for in terms of circumferential curvature in the cylindrical coordinate system. Leyrat-Maurin & Barthes-Biesel (1994) studied the motion of a deformable capsule surrounded by an infinitely thin Mooney–Rivlin membrane through a hyperbolic constriction. They reported that when the effective radius of the capsule is large enough, it can plug the constriction under either constant-flow-rate or constant-pressure-drop conditions. The effects of insoluble and soluble surfactant on the deformation and breakup of a drop in an extensional flow have been studied by Stone & Leal (1990), Milliken, Stone & Leal (1993) and Milliken & Leal (1994).

The case of a three-dimensional bubble or drop with constant surface tension moving in a straight or constricted capillary tube was recently studied by Tsai & Miksis (1994, referred to as TM hereafter). Assuming that the fluids were governed by the Stokes equations and using a boundary integral method, they determined numerically the dynamics of the drop or bubble as a function of the viscosity ratio (drop to suspending fluid) λ, capillary number and effective drop radius. The limit of $\lambda = 0$ or λ small is considered to be a bubble while large λ refers to a drop. Hence, depending on the value of λ, their results are applicable to either a drop or bubble. They found that in a straight capillary tube, small-capillary-number drops will approach a steady-state shape while large-capillary-number drops can have a jet of suspending fluid penetrating into the surface of the drop from the trailing interface. This result was also consistent with the experimental results of Olbricht & Kung (1992). For the case of a constriction, they found that when the viscosity ratio was small the bubble can break into two or more pieces, i.e. snap off. Otherwise the bubble just passed through the constriction. They also found that there was a finite range of capillary numbers for which the bubble would snap off. For small capillary numbers, the bubble just passed through the constriction while at larger capillary numbers, a thread of fluid at the rear of the bubble is observed as it passes through

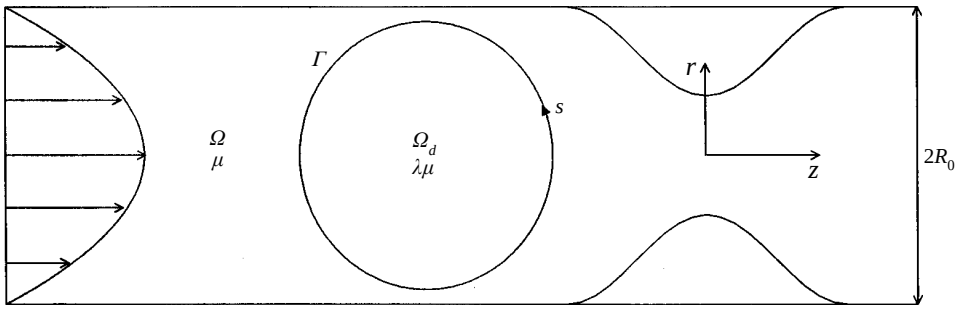

FIGURE 1. A bubble in a constricted capillary tube.

the constriction. Our aim in this work will be to expand on the work of Tsai & Miksis (1994) by including the effects of insoluble surfactant on the bubble surface. We will show how the presence of surfactant can affect the snap-off process and the dynamics of the bubble.

We note that one of the difficulties in studying these moving boundary problems arises from the nonlinearities in the boundary conditions on the fluid–fluid interface. Although the governing equations for the creeping motion are linear, the interface curvature is a nonlinear function of the coordinates of the drop shape. Furthermore, the time-dependent fluid–fluid interface is a free surface and has to be determined as part of the solution with the velocity and pressure fields, together with the surfactant distribution on the free surface. It has been shown that the boundary integral method is effective solving these problems numerically and it will be used here.

We begin with a formulation of the equations of motion in §2. Then in §3 we describe the numerical method used to compute the time-dependent drop evolution and the surfactant transport along the bubble surface. The dynamics of a bubble in both a straight and constricted capillary tube will be discussed in §4.

2. Formulation

Consider a neutrally buoyant Newtonian drop of undeformed radius a_0 and viscosity $\lambda\mu$, suspended in a straight or constricted circular capillary tube, filled with a second immiscible Newtonian fluid of viscosity μ. Both fluids are incompressible and the whole suspension is driven by an imposed pressure gradient such that the volume flux remains constant. At the fluid–fluid interface, the interfacial tension γ may vary with time and position along the interface owing to the presence of an adsorbed surface-active material. The surfactant is assumed to be insoluble in both the drop fluid and the suspending fluid so that convection and diffusion of surfactant in the bulk phases may be neglected. When the Reynolds numbers are small in both fluids so that the inertia terms can be neglected, the motions in both fluids are governed by the Stokes equations. Using the cylindrical coordinate system shown in figure 1, the governing equations in the suspending fluid $\boldsymbol{\Omega}$ are the conservation of mass and momentum

$$\nabla \cdot \boldsymbol{v} = 0, \tag{2.1a}$$

$$\mu \nabla^2 \boldsymbol{v} = \nabla P, \tag{2.1b}$$

for $\boldsymbol{x} \in \boldsymbol{\Omega}$, where $\boldsymbol{v}$ is the velocity and P is the pressure in the suspending fluid. Similarly, in the drop $\boldsymbol{\Omega}_d$, we have

$$\nabla \cdot \boldsymbol{v}_d = 0, \tag{2.2a}$$

$$\lambda\mu\nabla^2 \boldsymbol{v}_d = \nabla P_d, \tag{2.2b}$$

where $\boldsymbol{v}_d$ and P_d denote the velocity and pressure fields in the drop fluid, respectively.

The boundary condition for the velocities along the tube wall satisfies the no-slip condition

$$\boldsymbol{v} = 0. \tag{2.3}$$

Along the fluid–fluid interface Γ, the boundary conditions are the continuity of velocity

$$\boldsymbol{v} = \boldsymbol{v}_d, \tag{2.4}$$

the stress condition

$$\boldsymbol{\sigma}(\boldsymbol{v}) \cdot \boldsymbol{n} - \boldsymbol{\sigma}(\boldsymbol{v}_d) \cdot \boldsymbol{n} = \gamma(\nabla_s \cdot \boldsymbol{n})\boldsymbol{n} - \nabla_s \gamma, \tag{2.5}$$

and the kinematic condition

$$\frac{\partial \boldsymbol{Y}}{\partial t} \cdot \boldsymbol{n} = \boldsymbol{v} \cdot \boldsymbol{n}. \tag{2.6}$$

In these equations, $\boldsymbol{\sigma}(\boldsymbol{v}) = -P\boldsymbol{I} + \mu(\nabla \boldsymbol{v} + (\nabla \boldsymbol{v})^T)$ and $\boldsymbol{\sigma}(\boldsymbol{v}_d) = -P_d\boldsymbol{I} + \lambda\mu(\nabla \boldsymbol{v}_d + (\nabla \boldsymbol{v}_d)^T)$ are the stress tensors for the suspending and the drop fluids, respectively; ∇_s denotes the surface gradient, $\boldsymbol{n}$ is the unit normal vector pointed away from $\boldsymbol{\Omega}$, $\nabla_s \cdot \boldsymbol{n}$ is the mean curvature of the fluid–fluid interface, $\gamma(\tilde{C})$ is the interfacial tension which depends on the surfactant concentration $\tilde{C}$, and $\boldsymbol{Y}$ is the position vector of Γ. Furthermore, due to the presence of surfactant on the fluid–fluid interface, its distribution along the interface has to be coupled with the above boundary conditions on Γ. The changes in surfactant concentration at a phase interface are governed by a time-dependent convective–diffusion equation, which can be written as

$$\frac{\partial \tilde{C}}{\partial t} + \nabla_s \cdot (\tilde{C}\boldsymbol{v}_s) + (\nabla_s \cdot \boldsymbol{n})(\boldsymbol{v} \cdot \boldsymbol{n})\tilde{C} = D_s {\nabla_s}^2 \tilde{C}, \tag{2.7}$$

see Aris (1962) and more recently Stone (1990) for the derivation of equation (2.7), where D_s is the surface diffusivity and $\boldsymbol{v}_s$ represents the velocity vector tangent to the interface ($\boldsymbol{v}_s = (\boldsymbol{I} - \boldsymbol{nn}) \cdot \boldsymbol{v}$).

Finally, the velocity of the suspending fluid should approach Poiseuille flow when it is sufficiently far away from the drop and the constriction:

$$\boldsymbol{v} = \frac{2Q}{\pi R_0^4}(R_0^2 - r^2)\boldsymbol{e}_z \quad \text{as} \quad |z| \to \infty. \tag{2.8}$$

Here Q is the constant volume flux of the whole suspension, $\boldsymbol{e}_z$ is the unit vector along the axial direction, and r is the radial distance measured from the tube centreline.

In order to complete the formulation, an equation of state which relates the interfacial tension and the surfactant concentration must be described. Here we use a linear equation of state

$$\gamma_s - \gamma = \tilde{C}RT, \tag{2.9}$$

where γ_s is the interfacial tension of a clean interface (i.e. $\tilde{C} = 0$), R is the gas constant and T is the absolute temperature. The surfactant concentration $\tilde{C}$ is specified in units of mass of surfactant per unit of interfacial surface area. This simple equation of state is valid for a dilute surfactant concentration and has been used by other

researchers in studying the effects of surfactant on the deformation of drops, e.g. Stone & Leal (1990). As the surfactant concentration increases, a nonlinear equation would be more appropriate, e.g. a Frumkin model, but these require the specification of additional parameters. Hence for simplicity we will use the linear equation (2.9) here.

To non-dimensionalize the governing equations and boundary conditions, we choose the radius at the straight section of the capillary tube, R_0, as the length scale; the surfactant concentration is scaled by the uniform concentration C_0, which exists on the fluid–fluid interface in the absence of flow; the velocity is scaled by V, where $V = Q/\pi R_0^2$ represents the average velocity of the suspending fluid; the pressure is scaled by $\mu Q/\pi R_0^3$ and the time is scaled by $\pi R_0^3/Q$. The governing equations in dimensionless form become

$$\nabla \cdot \boldsymbol{v} = 0, \tag{2.10a}$$

$$\nabla^2 \boldsymbol{v} = \nabla P, \tag{2.10b}$$

for $\boldsymbol{x} \in \boldsymbol{\Omega}$. While in the drop, $\boldsymbol{x} \in \boldsymbol{\Omega}_d$,

$$\nabla \cdot \boldsymbol{v}_d = 0, \tag{2.11a}$$

$$\lambda \nabla^2 \boldsymbol{v}_d = \nabla P_d. \tag{2.11b}$$

The dimensionless boundary conditions along the tube wall become

$$\boldsymbol{v} = 0 \quad \text{at} \quad r = w(z) \quad \text{for} \quad -\infty < z < \infty \tag{2.12}$$

where $w(z)$ describes the shape of the capillary tube wall. At the fluid–fluid interface Γ, the boundary conditions are

$$\boldsymbol{v} = \boldsymbol{v}_d, \tag{2.13}$$

$$\boldsymbol{\sigma}(\boldsymbol{v}) \cdot \boldsymbol{n} - \boldsymbol{\sigma}(\boldsymbol{v}_d) \cdot \boldsymbol{n} = \frac{1}{Ca}(1 - \beta C)(\nabla_s \cdot \boldsymbol{n})\boldsymbol{n} + \frac{\beta}{Ca}\nabla_s C, \tag{2.14}$$

$$\frac{\partial \boldsymbol{Y}}{\partial t} \cdot \boldsymbol{n} = \boldsymbol{v} \cdot \boldsymbol{n}. \tag{2.15}$$

The convective–diffusion equation for the surfactant concentration becomes

$$\frac{\partial C}{\partial t} + \nabla_s \cdot (C\boldsymbol{v}_s) + (\nabla_s \cdot \boldsymbol{n})(\boldsymbol{v} \cdot \boldsymbol{n})C - \frac{1}{Pe}\nabla_s^2 C = 0. \tag{2.16}$$

Finally

$$\boldsymbol{v} = 2(1 - r^2)\boldsymbol{e}_z \quad \text{for } |z| \to \infty,\ 0 \leqslant r \leqslant 1 \tag{2.17}$$

at the upstream and downstream boundaries. Here we have introduced the dimensionless parameters

$$Ca = \frac{\mu Q}{\pi R_0^2 \gamma_s}, \quad \beta = \frac{C_0 RT}{\gamma_s}, \quad \text{and} \quad Pe = \frac{R_0 V}{D_s}.$$

Ca is the capillary number based on the interfacial tension of a clean fluid–fluid interface, β is a physicochemical parameter that determines the sensitivity of the interfacial tension to changes in surfactant concentration, and Pe is the surface Péclet number. The capillary number is the appropriate dimensionless measure of viscous forces relative to interfacial tension forces. The surface Péclet number is a measure of relative importance of convection to diffusion. In addition to these parameters, we have two more physical parameters in the formulation: the effective radius of the drop $a = a_0/R_0$ and the viscosity ratio λ.

As noted by Stone & Leal (1990), the dimensional interfacial tension in the presence of a (non-dimensional) surfactant concentration becomes

$$\gamma = \gamma_s(1 - \beta C). \tag{2.18}$$

Hence in the absence of flow, a uniform surfactant concentration, $C = 1$, decreases the interfacial tension to $\gamma = \gamma_s(1 - \beta)$. This shows that β is bounded by $0 \leqslant \beta \leqslant 1$. Furthermore, this suggests an appropriate scale for the capillary number, which is based upon the equilibrium interfacial tension $\gamma_s(1 - \beta)$. Therefore, we define the normalized capillary number as $Ca^* = Ca/(1 - \beta)$. This is the capillary number based upon the equilibrium interfacial tension due to the uniform concentration of surfactant in the absence of flow. Thus Ca^* is the appropriate parameter for the study of the deformation of a drop due to surfactant variations by the imposing flow fields.

The shape of the capillary tube wall is specified by the function $w(z)$, where

$$\left.\begin{array}{ll} w(z) = 1 - d(1 + \cos(\pi z/l)) & \text{for} \quad -l < z < l \\ w(z) = 1 & \text{otherwise.} \end{array}\right\} \tag{2.19}$$

Note that the centre of the constriction is located at the origin and we have introduced two geometrical parameters for the constriction shape, $2d$ and $2l$, which determine its depth and length, respectively.

Starting with an initially spherical bubble with a uniform surfactant concentration, our goal is to solve equations (2.10)–(2.11) subject to the boundary conditions (2.12)–(2.17). Although analytical solutions for this free boundary problem coupled with the surfactant transport equation are difficult to obtain in general, numerical methods which utilize the boundary integral method are an effective way of solving this set of problems. In the next section, we outline the numerical procedure used to determine the time-dependent solutions for the surfactant concentrations on the deforming surface of the bubble or drop as it travels in a straight or constricted capillary tube.

3. Numerical method

In this section, we discuss the numerical procedure to solve this coupled free-boundary and surfactant transport problem. The boundary integral equations for a clean fluid–fluid interface, where the interfacial tension is assumed to be constant, are given in TM. When surfactant is present at the interface, we can write the following boundary integral equations for the surface velocities and tractions assuming a linear equation of state (2.18):

$$(1+\lambda)C_{ki}v_i(\boldsymbol{x})+(1-\lambda)\int_{\Gamma} T_{ik}(\boldsymbol{x},\boldsymbol{y})v_i(\boldsymbol{y})\mathrm{d}\Gamma+\int_{\Gamma_w} T_{ik}(\boldsymbol{x},\boldsymbol{y})v_i(\boldsymbol{y})\mathrm{d}\Gamma_w$$

$$-\int_{\Gamma_w} U_{ik}(\boldsymbol{x},\boldsymbol{y})t_i(\boldsymbol{v}(\boldsymbol{y}))\mathrm{d}\Gamma_w=\int_{\Gamma} U_{ik}(\boldsymbol{x},\boldsymbol{y})\left[\frac{1-\beta C}{Ca}(\nabla\cdot\boldsymbol{n})n_i(\boldsymbol{y})+\frac{\beta}{Ca}\nabla C\right]\mathrm{d}\Gamma, \tag{3.1}$$

for $\boldsymbol{x} \in \Gamma$, and

$$C_{ki}v_i(\boldsymbol{x}) + (1-\lambda)\int_{\Gamma} T_{ik}(\boldsymbol{x},\boldsymbol{y})v_i(\boldsymbol{y})\mathrm{d}\Gamma + \int_{\Gamma_w} T_{ik}(\boldsymbol{x},\boldsymbol{y})v_i(\boldsymbol{y})\mathrm{d}\Gamma_w$$

$$-\int_{\Gamma_w} U_{ik}(\boldsymbol{x},\boldsymbol{y})t_i(\boldsymbol{v}(\boldsymbol{y}))\mathrm{d}\Gamma_w=\int_{\Gamma} U_{ik}(\boldsymbol{x},\boldsymbol{y})\left[\frac{1-\beta C}{Ca}(\nabla\cdot\boldsymbol{n})n_i(\boldsymbol{y})+\frac{\beta}{Ca}\nabla C\right]\mathrm{d}\Gamma, \tag{3.2}$$

for $\boldsymbol{x} \in \Gamma_w$. In these equations, C_{ki} is the principal value tensor, which depends on the smoothness of the boundary and can be found in Martinez & Udell (1990), $\boldsymbol{y}$ is the integration variable, $\boldsymbol{n}$ is the unit normal vector pointed away from $\boldsymbol{\Omega}$, and $t_i(\boldsymbol{v}(\boldsymbol{y})) = \boldsymbol{\sigma}_{ik} n_k$ is the tractions. The boundary Γ_w includes the capillary wall plus an upstream and downstream computational boundary taken far away from the drop and the constriction. The kernels of the integral equations are known functions of position given by

$$U_{ik}(\boldsymbol{x}, \boldsymbol{y}) = \frac{-1}{8\pi} \left\{ \frac{\delta_{ik}}{| \boldsymbol{x} - \boldsymbol{y} |} + \frac{(x_i - y_i)(x_k - y_k)}{| \boldsymbol{x} - \boldsymbol{y} |^3} \right\},$$

and

$$T_{ik}(\boldsymbol{x}, \boldsymbol{y}) = \frac{-3}{4\pi} \frac{(x_i - y_i)(x_j - y_j)(x_k - y_k)}{| \boldsymbol{x} - \boldsymbol{y} |^5} n_j(\boldsymbol{y}).$$

Assuming the motion is axisymmetric, the surface integrals in the above equations can be reduced to line integrals along the generating curve of the boundary by performing the azimuthal integrations analytically. The convective–diffusion equation can be written as

$$\frac{\partial C}{\partial t} + \frac{1}{r[(\partial r/\partial s)^2 + (\partial z/\partial s)^2]^{1/2}} \left\{ \frac{\partial}{\partial s}(C r v_s) - \frac{1}{Pe} \frac{\partial}{\partial s} \left[\frac{r}{[(\partial r/\partial s)^2 + (\partial z/\partial s)^2]^{1/2}} \frac{\partial C}{\partial s} \right] \right\}$$
$$+ C(\nabla \cdot \boldsymbol{n})(\boldsymbol{v} \cdot \boldsymbol{n}) = 0, \quad (3.3)$$

where the drop surface is parameterized using a surface coordinate (s, θ), θ is the azimuthal angle ($0 \leqslant \theta \leqslant 2\pi$) and s is the arclength coordinate measured from the front of the drop. Since the interface is deforming, the total arclength $L(t)$ is time-dependent. The velocity tangent to the surface v_s can be calculated once the boundary integral equations are solved, $v_s = \boldsymbol{v} \cdot \boldsymbol{t}$ where $\boldsymbol{t}$ is the unit tangent vector on the drop surface.

The axisymmetric version of the boundary integral equations (3.1)–(3.2) and the convective–diffusion equation (3.3) are discretized and solved numerically using the boundary integral method described in TM in conjunction with an implicit backward Euler scheme for the surfactant transport on the drop surface. The numerical method parallels the method used by Stone & Leal (1990). The surfactant concentration C is discretized using the same boundary nodes that describe the drop surface and is assumed to vary quadratically between nodal points. The boundary conditions imposed for equation (3.3) are $\partial C/\partial s = 0$ at $s = 0$ and $s = L(t)$. The resulting tridiagonal linear system of equations is solved using the LAPACK routine DGTSV with double precision.

We summarize the numerical algorithm for solving the transient motion of a drop in a capillary tube with surfactant transport on a deforming drop surface as follows:

(*a*) For a given drop shape and surfactant concentration at time t, compute the interfacial velocity field from equations (3.1) and (3.2), and update the drop shape to time $t + \Delta t$ using equation (2.15) with a second-order Runge–Kutta scheme.

(*b*) Using the drop shape at time $t + \Delta t$ and the interfacial velocity field obtained from the last step of the second-order Runge–Kutta scheme in (*a*), update the surfactant concentration from time t to $t + \Delta t$ using equation (3.3).

(*c*) Redistribute the nodal points along the drop shape at time $t + \Delta t$ in terms of an equally spaced arclength coordinate and interpolate the surfactant concentration at the new nodal points.

(*d*) Return to step (*a*).

Boundary conditions far away from the drop and the constriction require that the fluid velocity approaches the Poiseuille velocity profile. To achieve this numerically, we impose a Poiseuille flow at the downstream boundary, while at the upstream boundary we set the radial component of the flow and the normal stress to zero. For additional details, see Tsai (1994).

A spherical drop with uniform surfactant concentration ($C = 1$) is used to initiate this procedure. In order to have a fixed computational domain for the translation of the drop in a straight capillary tube, the computations are carried out with the nose of the drop placed at the origin. Thus, at the end of each iteration, the drop shape is shifted backward uniformly by an amount equal to the axial displacement of the nose. For the case of a constricted capillary tube, the nose of the bubble is placed at $z = -(l + 0.1)$ at time $t = 0$ on the upstream side of the constriction, and the computations are terminated when snap-off occurs. Snap-off is defined to be the instant in time when the minimum radial coordinate of the boundary nodes on the bubble surface in the neighbourhood of the constriction is less than 0.02, and this point will be called the snap-off point. The predicted snap-off time τ is defined to be the difference between the two instants in time when the nose of the bubble passes the centre of the constriction and the time when the snap-off criterion is satisfied. Assuming that the bubble breaks at the snap-off point, the effective radius of the bubble generated, b_r, is computed by using a flat trailing interface which connects the snap-off point to the axial axis. The effective radius b_r is defined to be the radius of a spherical bubble with the same volume as the bubble being generated at the downstream side of the constriction.

The convergence of the numerical scheme described above is illustrated by simultaneously doubling the number of boundary nodes and halving the time step Δt of the numerical integration in (2.15) while keeping the ratio of Δs and Δt fixed. Here Δs denotes the arclength between two successive grid points along the drop surface. On doing this, the numerical results show convergent bubble shapes and surfactant concentration throughout the time evolution up to the occurrence of bubble snap-off when the computations are terminated. Since the fluids are incompressible and the surfactant is assumed to be insoluble, the volume of the bubble and the total amount of surfactant should remain constant throughout the time evolution. Hence, it is convenient to monitor these two quantities as a check of the accuracy of the numerical scheme. It is found that in order to capture the snap-off phenomena accurately, a minimum number of boundary nodes on the bubble surface, depending on the value of the dimensionless parameters, is needed. For example, starting from 11 nodes on the upstream and downstream computational boundaries, located at the axial coordinates -6 and 6, together with 81 nodes along the tube wall, and 61 nodes on the bubble surface, with the corresponding time step $\Delta t = 0.002$, we find that for a bubble of $a = 0.9$ and $\lambda = 10^{-3}$, and for the dimensionless parameters $Ca^* = 0.1$, $\beta = 0.5$, and $Pe = 1$, the computations performed up to the instant of bubble snap-off, $t = 0.492$, have lost 9.19% of bubble volume. Doubling the number of nodes gives at $t = 0.492$ a 2.40% decrease of bubble volume while doubling again gives a 0.71% decrease. Correspondingly, the percent change in the total amount of surfactant at time $t = 0.492$ decreases from 0.596%, to 0.189%, and then to 0.069%. The pressure jump across the capillary tube has a maximum and a minimum as a function of time during the passage of the bubble through the constriction up to $t = 0.492$ and the corresponding values for these are 337.7, 327.7, 326.1, for the maximum, and 195.3, 177.5, 173.6, for the minimum, as the meshes are refined. These results imply approximately second-order convergence for the numerical algorithm described above.

During the evolution of the bubble, the upstream and downstream computational boundaries are taken at least R_0 units away from the bubble and constriction. We have also checked that increasing the size of the upstream and downstream computational boundaries has no discernible effects on our results. Unless otherwise noted, the error in bubble volume is less than 1.5% from its initial volume, and the error in total surfactant concentration is less than 1% from the total surfactant concentration at time $t = 0$. Hence, we are confident that the numerical results presented here are all within graphical accuracy.

4. Results and discussion

Our numerical results are presented in this section. First we consider the effects of surfactant on the motion of a drop in a straight capillary tube. Then the effects of surfactant on the dynamics of a bubble in a constricted capillary tube are considered. The initial drop shape for all of the computations presented in this section is a sphere with effective radius $a = 0.9$, and with a uniform surfactant concentration of $C = 1$. We should note that in TM, the dynamics of drops with constant interfacial tension at larger values of a were found to be similar to the case of $a = 0.9$. We also note once again that the computations presented here use the linear equation of state (2.9) and hence the results may differ from predictions using a nonlinear equation of state.

4.1. *Straight capillary*

In their study on the dynamics of a drop with constant interfacial tension in a straight capillary tube, TM showed that for small values of the capillary number Ca, steady-state drop shapes exist. But as its value increased, a critical value of Ca is reached at which the steady-state drop profiles no longer exist. In particular, they presented solutions for which a jet of suspending fluid penetrated into the surface of the drop from the trailing interface. In the presence of surfactant, we find that the motion of a drop can be similarly described if we use the normalized capillary number, Ca^*, instead of Ca. As we will show, for small values of Ca^* the drops will approach steady-state shapes, but the dynamics becomes more complicated at larger values of Ca^*. In our computations, we say that a drop in a straight capillary tube has reached its steady-state shape when the computed axial velocities at the front and rear poles of the drop are within 1% of each other. Only the $\lambda = 0.1$ case will be studied here. As shown in TM, similar behaviour was found for smaller values of λ.

In figure 2 we present computed steady-state solutions for $Ca = 0.1$, $Pe = 1$ and $\beta = 0.1, 0.2, 0.5, 0.75$. The corresponding values of Ca^* are 0.111, 0.125, 0.2 and 0.4, respectively. Figure 2(a) shows the computed steady-state drop profiles plotted with their noses located at $z = 0$. We can see that as β increases, the steady-state drop profiles elongate in the axial direction and decrease in radius in the radial direction. Hence, as β increases, the curvature at the front of the drop increases while the trailing interface initially flattens but then eventually, for large enough β, a re-entrant cavity at the trailing interface appears. In TM a similar phenomenon occurred with increasing capillary number. Additional insight can be obtained by examining the steady-state surfactant concentration, C, on the drop surfaces, shown in figure 2(b), and the corresponding interfacial tension, γ/γ_s, shown in figure 2(c). These dependent variables are plotted as a function of z. For the case of $\beta = 0.75$, we see that the surfactant concentrations are nearly uniform along the rear interface of the drop. The degree of drop deformation is directly related to the interfacial tension forces on its

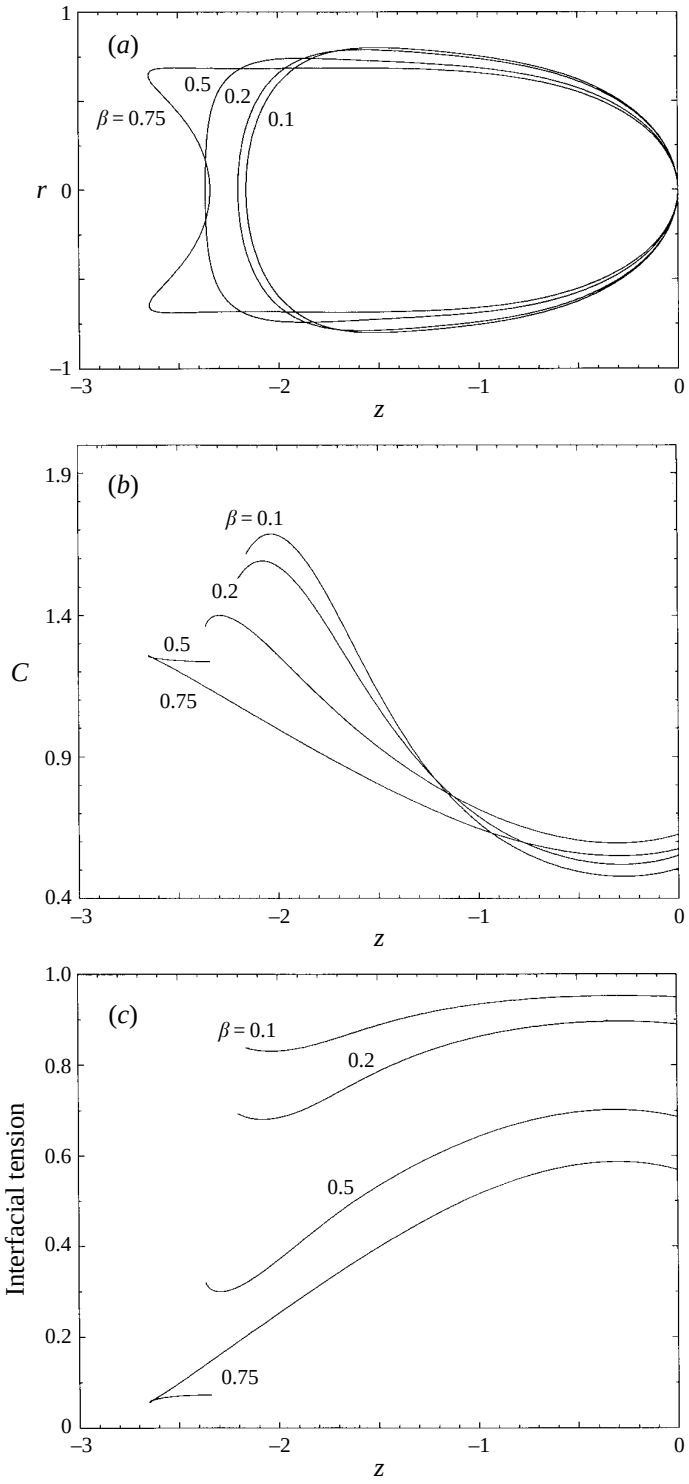

FIGURE 2. (*a*) Steady drop shape, (*b*) surfactant concentration and (*c*) interfacial tension forces γ/γ_s, for $Ca = 0.1$, $Pe = 1$, and $\beta = 0.1, 0.2, 0.5$, and 0.75.

surface. In figure 2(*c*), we find that the interfacial tension on the drop surface decreases with increasing β, therefore requiring an increased deformation of the drop shape in the neighbourhood of the wing tips with increasing β. Similar steady-state drop shapes for other values of the dimensionless parameters were obtained by Borhan & Mao (1992).

For the case of $\beta = 0.75$, we should note that the change in the total amount of surfactant was around 5.5% when the steady-state criterion was satisfied. The increase of error in this case is associated with a large variation of curvature at the tip of the cavity on the rear interface of the drop. Because of the development of this large curvature, the spatial derivative of the surface velocity field also increases in magnitude in order to satisfy the stress boundary condition (2.14), which, in turn, results in the formation of a spike in $\partial^2 C/\partial s^2$ at the tip of the cavity. Increasing the number of boundary nodes on the drop surface makes the drop shape smoother and the spike in $\partial^2 C/\partial s^2$ more localized. Hence, the surfactant concentration profile for this case has a large gradient in its derivative at the tip of the cavity due to the development of a large curvature.

As the value of Ca^* increases, the drop undergoes a larger deformation owing to the increase of viscous forces. The results of our computations indicate that a steady-state drop shape may no longer exist for large enough Ca^* due to the coupled effects of the accumulation of surfactant and the development of a re-entrant cavity at the trailing interface. In figure 3, we set $Ca^* = 1$, $\beta = 0.5$, and $Pe = 0.1, 1, 10$, and plot the drop shapes at time $t = 0.8$ in figure 3(*a*), and the corresponding surfactant concentration on the drop surface in figure 3(*b*). In figure 3(*a*), we also plot the drop shape at time $t = 0.8$ where a uniform surfactant concentration is maintained on the drop surface ($Ca = 1, \beta = 0$). It should be noted that in figure 3(*b*), the surfactant concentration is plotted as a function of arclength s along the drop surface, where $s = 0$ denotes the nose of the drop (see figure 1). When the Péclet number increases the effects of surface convection increase and we find that this leads to large variations in the surfactant concentration. In particular, as shown in figure 3(*b*), the accumulation of surfactant on the rear interface increases with increasing Péclet number. Therefore the surface tension decreases in the neighbourhood of the wing tips and an increased deformation occurs in order to satisfy the normal stress balance. Also the surface gradient of C increases at the wing tips so by (2.14) the jump in the tangential stress must also increase there. Both of these lead to the increase in the extent of penetration of the re-entrant cavity at the rear interface. In figure 3(*c*) we plot the tangential surface velocity for the drops of figure 3(*a*). Note the similarity in all of the curves. In particular, we find very little difference in the drop shapes near the nose but there is an increase of the tangential velocity with increasing Péclet number at the rear pole. In the neighbourhood of the wing tips, we find only small variations of the tangential velocity yet a larger value of concentration as Péclet number increases.

If time were allowed to increase, the uniform-surfactant case would have a jet of suspending fluid enter from the trailing interface of the drop and this eventually leads to drop breakup (see TM). When surfactant is present, we find with increasing time that there is accumulation of surfactant and increasing curvature and velocity gradients at the tip of the re-entrant cavity which leads to increased penetration of the re-entrant cavity. These effects make it difficult for the numerical computation to resolve the drop motion accurately for large time. But the results imply that the small-Pe cases should parallel the unsteady motion of the uniform-surfactant case but the larger-Pe cases contain additional dynamics beyond what we can accurately capture with our numerical method.

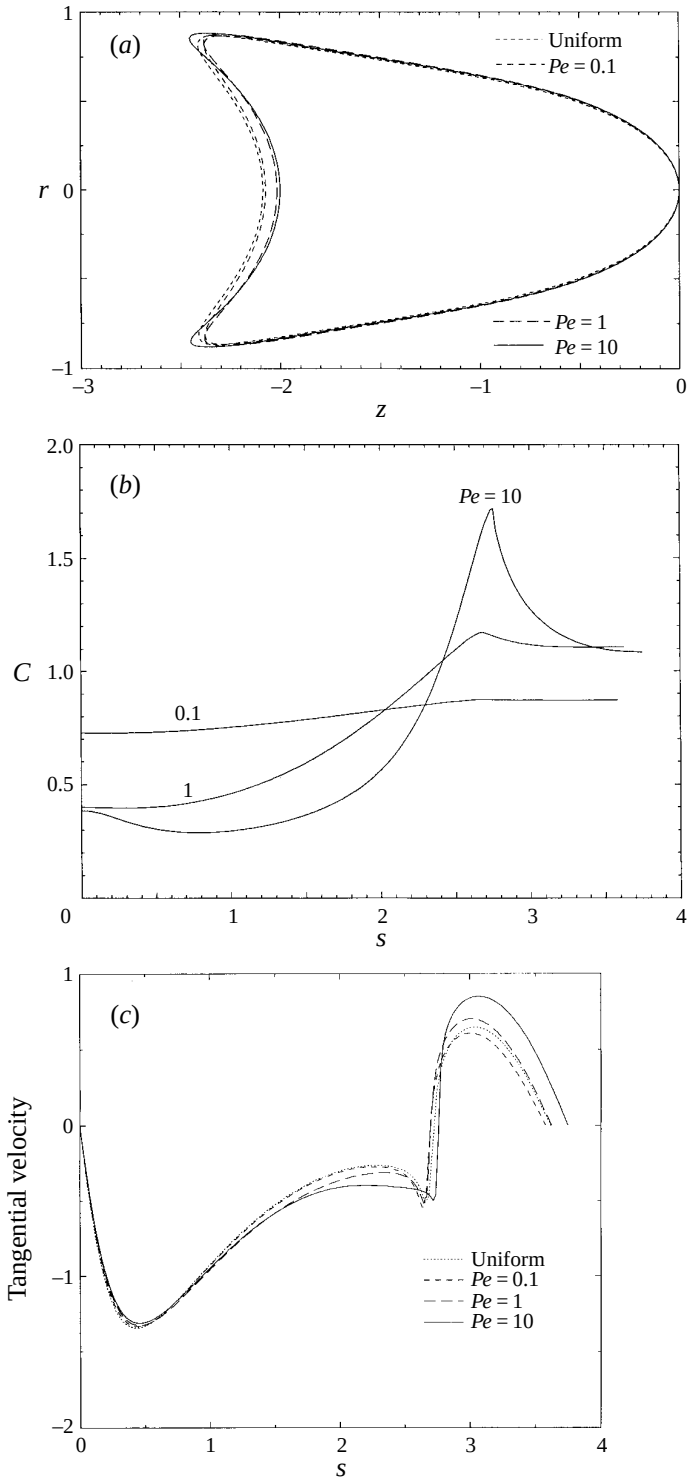

FIGURE 3. (*a*) Unsteady drop deformations, (*b*) surfactant concentration and (*c*) tangential surface velocity, at time $t = 0.8$ for $Ca^* = 1$, $\beta = 0.5$, and $Pe = 0.1, 1, 10$. In (*a*) $\beta = 0$ is also shown.

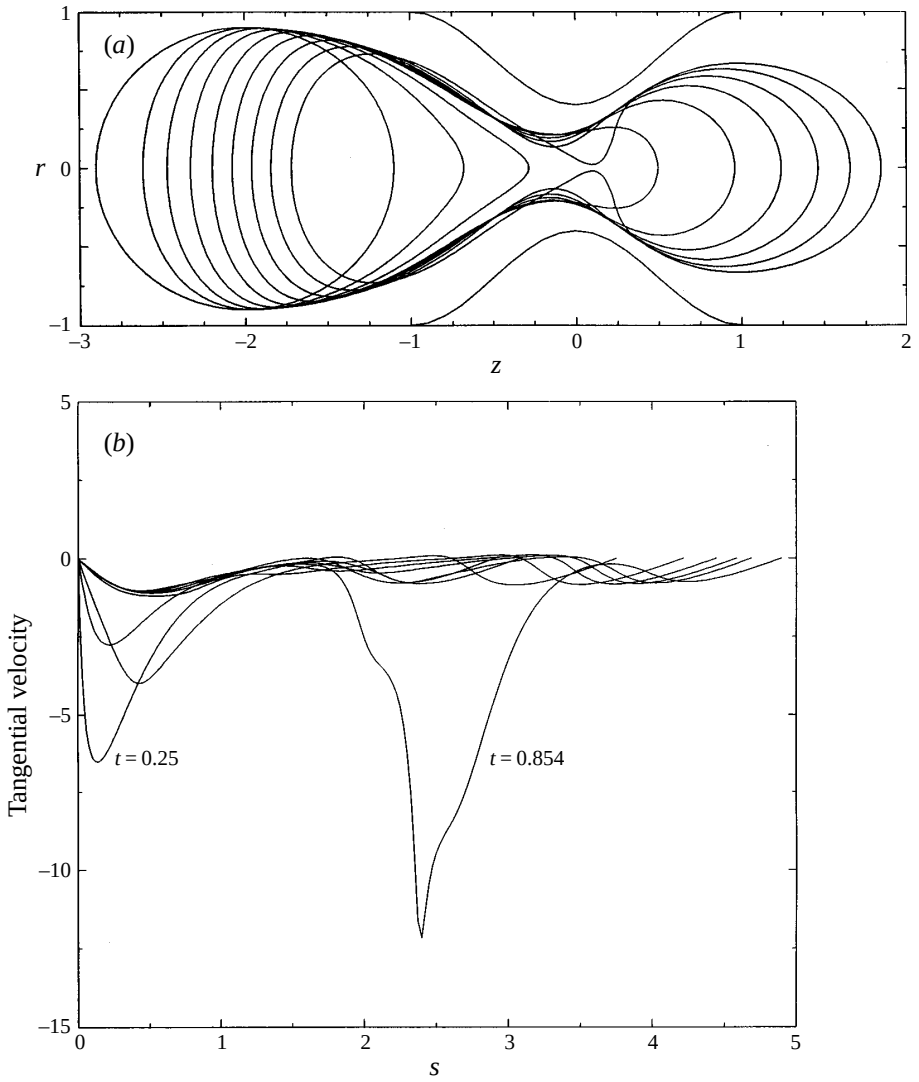

FIGURE 4. (*a*) Evolution of a clean bubble with constant surface tension. The initial shape is a sphere and $Ca^* = Ca = 0.1$. Plots are at times 0, 0.15, 0.25, 0.35, 0.45, 0.55, 0.65, 0.75, and 0.854. (*b*) As (*a*) but tangential surface velocity.

4.2. *Constricted capillary*

The effects of surfactants on the dynamics of bubble snap-off in a constricted capillary tube are now considered. It was shown in TM that for a given constriction shape, bubble snap-off occurs for a clean bubble surface (or a uniformly contaminated surface without surfactant transport) when the viscosity ratio λ is small. In addition, we also showed in TM that the effects of changing the effective bubble radius and the initial bubble shape result in only quantitative but not qualitative differences in the overall dynamics. So we will only use bubbles with the effective radius $a = 0.9$ and $\lambda = 10^{-3}$ in the numerical computations to demonstrate the effects of non-uniform surfactant concentration on the dynamics of bubble snap-off. The shape of the constriction is specified by setting $d = 0.3$ and $l = 1$.

In order to give us a better understanding of the effect of surfactant, in figure 4 we plot the bubble shape and the tangential velocity along the surface for a clean bubble, i.e. $Ca = Ca^* = 0.1$ and $\beta = 0$. The dimensionless times for the plots in figure 4 correspond to $t = 0, 0.15, 0.25, 0.35, 0.45, 0.55, 0.65, 0.75, 0.854$. The snap-off time is $\tau = 0.563$, while the effective radius is $b_r = 0.7193$. From figure 4(b) we see that the magnitude of the tangential velocity initially increases in the neighbourhood of the bubble nose as the bubble enters the constriction. Then as the bubble starts to come out of the constriction and expand, the magnitude of the tangential velocity remains relatively uniform in the neighbourhood of the nose but increases in the neighbourhood of the snap-off point. Hence if surfactant were present, an accumulation of surfactant would be expected at the snap-off point.

The variation of the surfactant concentration on the bubble surface is strongly influenced by the magnitude of the Péclet number, the dimensionless measure of the relative importance of surface convection to surface diffusion. As Péclet number increases, the surface convection becomes dominant and we could expect a large variation in the surfactant concentration. Here we will examine the bubble shapes and the corresponding surfactant concentration on the bubble surface for different values of the Péclet number. In figures 5 to 7, we plot the bubble shapes, the corresponding surfactant concentration and the tangential surface velocities as a function of arclength s for the evolution of an initially spherical bubble moving past a constriction and snapping off a smaller bubble, for the dimensionless parameter $Ca^* = 0.1$, $\beta = 0.5$, and $Pe = 0.1, 1, 100$, respectively. The dimensionless times chosen for the plots in figure 5 correspond to $t = 0.15, 0.25, 0.3, 0.35, 0.4, 0.6175$ for $Pe = 0.1$. The snap-off time is $\tau = 0.318$ and the effective radius $b_r = 0.5619$. The dimensionless times chosen for the plots in figure 6 correspond to $t = 0.15, 0.25, 0.3, 0.35, 0.4, 0.502$ for $Pe = 1$, and in this case $\tau = 0.2165$ and $b_r = 0.4584$. The dimensionless times chosen for the plots in figure 7 correspond to $t = 0.15, 0.25, 0.3, 0.35, 0.4, 0.4335$ for $Pe = 100$, and in this case $\tau = 0.1765$ and $b_r = 0.3897$. Clearly as Péclet number is increased, the snap-off time and effective radius decrease. In addition we see that surfactant concentration increases in the neighbourhood of the snap-off point with increasing Pe. When $Pe = 0.1$, surface diffusion is the dominant mechanism for the surfactant transport and we find that the surfactant concentration is fairly uniform for each bubble shape until the front of the bubble reaches the centre of the constriction. As the front of the bubble passes the centre of the constriction and enters the diverging section, the surfactant concentration at the front of the bubble starts decreasing owing to the increase in the interfacial surface area at the bubble front as it expands. Although the variations in the surfactant concentration in this case are minimal (compared to large values of Pe), nonetheless the presence of non-uniform surfactant concentration has accelerated the snap-off process in comparison to the case where a uniform surfactant concentration is maintained on the bubble surface throughout the bubble evolution. As Péclet number increases we find large variations in the surfactant concentration on the bubble surface. We also see in figures 5–7 that the value of C increases at the nose, as t increases up to 0.25, and then decreases. This local maximum of C increases with Pe. The initial increase in C at the front of the bubble follows because as the front of the bubble enters the converging section of the constriction, surfactant accumulates at the front of the bubble due to the converging flow fields as a result of the wall geometry. The amount of surfactant that accumulates at the front of the bubble increases with increasing Péclet number since as Pe increases the effects of convection in (2.14) increase. Note from figures 4(b), 5(c), 6(c), and 7(c) that near the snap-off point all the surface velocity plots

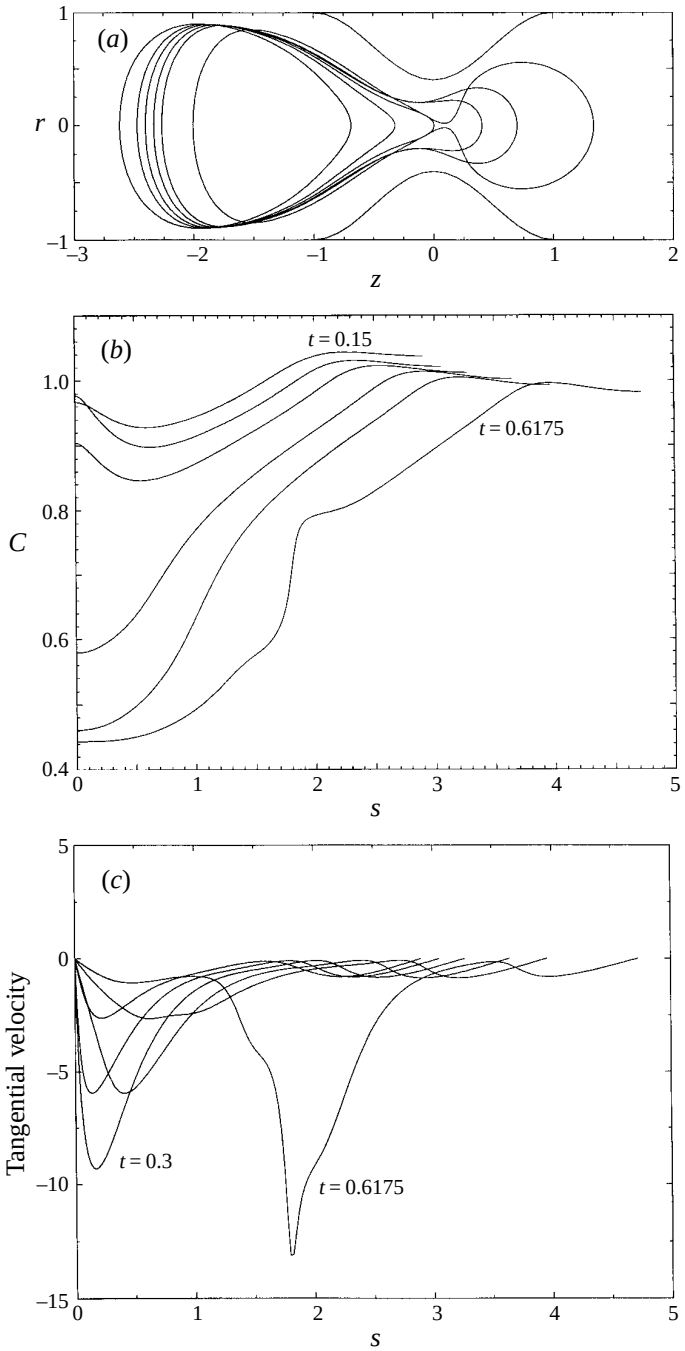

FIGURE 5. (*a*) Evolution of an initially spherical bubble with uniform surfactant concentration, (*b*) surfactant concentration, and (*c*) tangential surface velocity, for $Ca^* = 0.1$, $\beta = 0.5$, and $Pe = 0.1$, at times 0.15, 0.25, 0.3, 0.35, 0.4, and 0.6175.

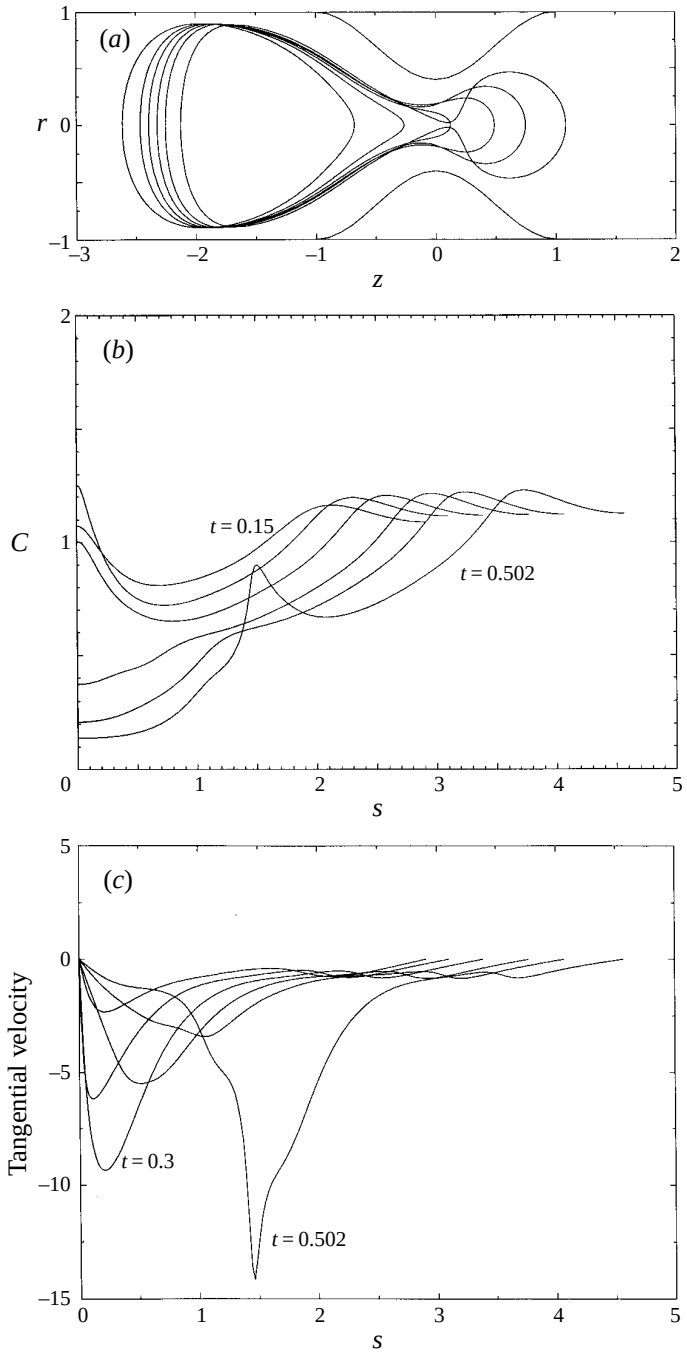

FIGURE 6. (*a*) Evolution of an initially spherical bubble with uniform surfactant concentration, (*b*) surfactant concentration and (*c*) tangential surface velocity, for $Ca^* = 0.1$, $\beta = 0.5$, and $Pe = 1$, at times 0.15, 0.25, 0.3, 0.35, 0.4, and 0.502.

are similar except for the fact that they occur earlier in time as Pe increases. Also note that the interfacial tension gradients resulting from the non-uniform surfactant concentration increase more rapidly in time with increasing Péclet number.

So why do the snap-off time and b_r decrease when surfactants are present? Putting together all of the above observations the following set of steps seems to take place. First we find that as a result of the initial increase in C, the local interfacial tension forces at the front of the bubble decrease requiring increased deformations (increased curvatures) to satisfy the normal stress balance. Hence the radius of the initial jet of liquid from the bubble passing through the constriction is less since the larger curvature of the nose allows for a narrower jet. The narrower jet moves faster through the constriction since it is further away from the walls. Once the front of the bubble reaches the diverging section of the constriction, the bubble starts expanding out of the constriction and the amount of surfactant at the front of the bubble starts decreasing due to the increase in the interfacial surface area as the bubble expands. This triggers the snap-off process. Since this all occurs faster than for a clean bubble, the snap-off time is less.

So why do the snap-off time and b_r decrease with increasing Pe? This is consistent with the fact that with increasing Pe the initial increase in C at the bubble nose also increases allowing for a larger curvature at the bubble nose. Hence the initial jet of liquid from the bubble moves quicker through the constriction but with a narrower radius so less fluid passes through the constriction before we start to see the front expand and hence the snap-off time decreases with increasing Pe. For $Pe = 100$, it is also interesting to note that the snap-off point is shifted further downstream from the centre of the constriction compared to the case when the Péclet number is 0.1 and 1.

In figures 8(a) and 8(b), we plot the snap-off time and the effective radius b_r as a function of Péclet number for $Ca^* = 0.05, \beta = 0.7$; $Ca^* = 0.1, \beta = 0.5$; and $Ca^* = 0.15, \beta = 0.3$. For the case of $Ca^* = 0.05$ and $\beta = 0.7$, when the Péclet number is small, e.g. $Pe = 0.01$, surface diffusion renders the surfactant concentration profile almost uniform; the surfactant concentration on the bubble surface is slightly less than the initial concentration ($C = 1$) due to the increase in the surface area as the bubble deforms. Therefore the bubble passes through the constriction without snapping off and attains a steady-state shape downstream of the constriction. This is consistent with the results reported in TM. For the case of $Ca^* = 0.15$ and $\beta = 0.3$, when the Péclet number is large, e.g. $Pe = 100$, no bubble snap-off was observed up to time $t = 1.25$. This is significantly larger than the total evolution time for the case of $Pe = 10$, where we observe bubble snap-off at time $t = 0.463$. In addition, we should note that for the case of $Pe = 100$, the change in the total amount of surfactant was about 5.6% at time $t = 1.25$. This increase in the total amount of surfactant is similar to what had been noted earlier in the straight tube case, i.e. the coupled effects of the development of large curvature and the accumulation of surfactant on the bubble surface. For this case, we observe that surfactant accumulates at two locations on the bubble surface. As the front of the bubble expands out of the diverging section of the constriction, surfactant accumulates at the end of the expanding front interface near the minimum bubble radius and also near the rear interface, which is still on the upstream region of the constriction. Hence there is an increase in curvature at these locations on the bubble surface. The amount of surfactant that accumulates near the rear interface is larger than the amount of surfactant that accumulates at the end of the expanding front. As time increases further, the accumulation of surfactant at the rear interface keeps increasing, hence the interfacial tension forces on the rear

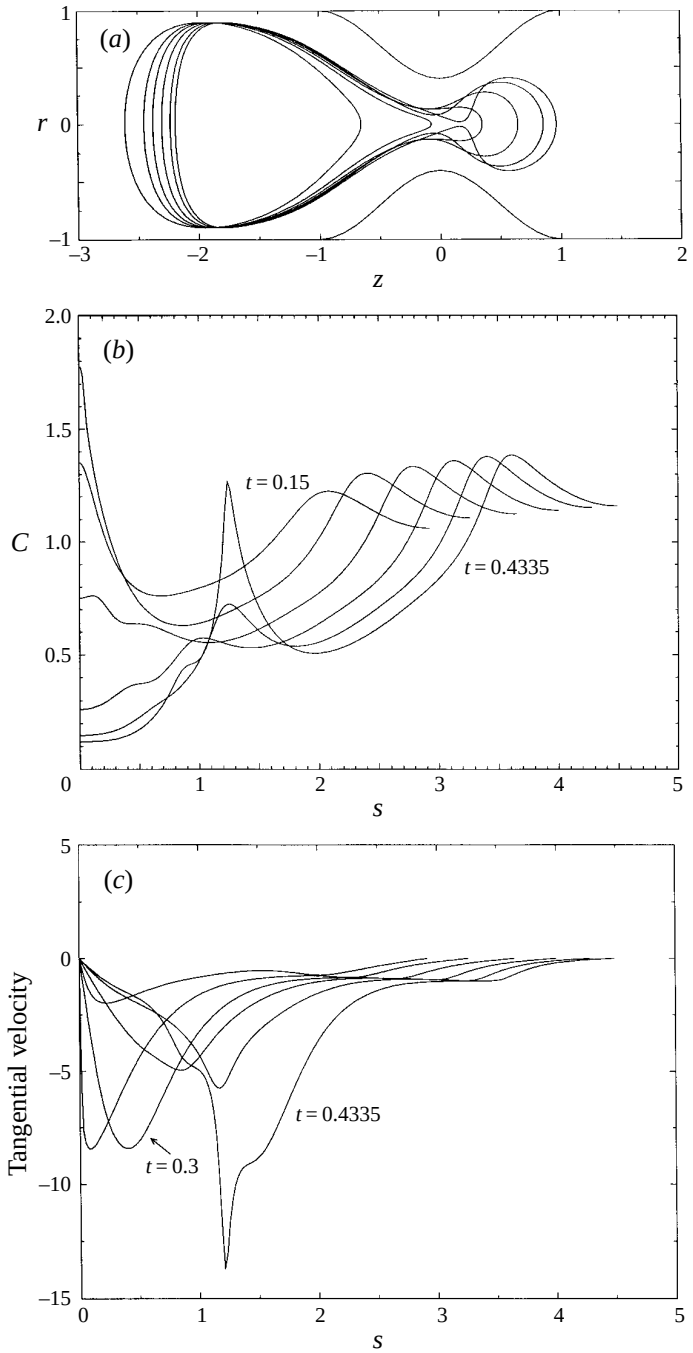

FIGURE 7. (*a*) Evolution of an initially spherical bubble with uniform surfactant concentration, (*b*) surfactant concentration and (*c*) tangential surface velocity, for $Ca^* = 0.1$, $\beta = 0.5$, and $Pe = 100$, at times 0.15, 0.25, 0.3, 0.35, 0.4, and 0.4335.

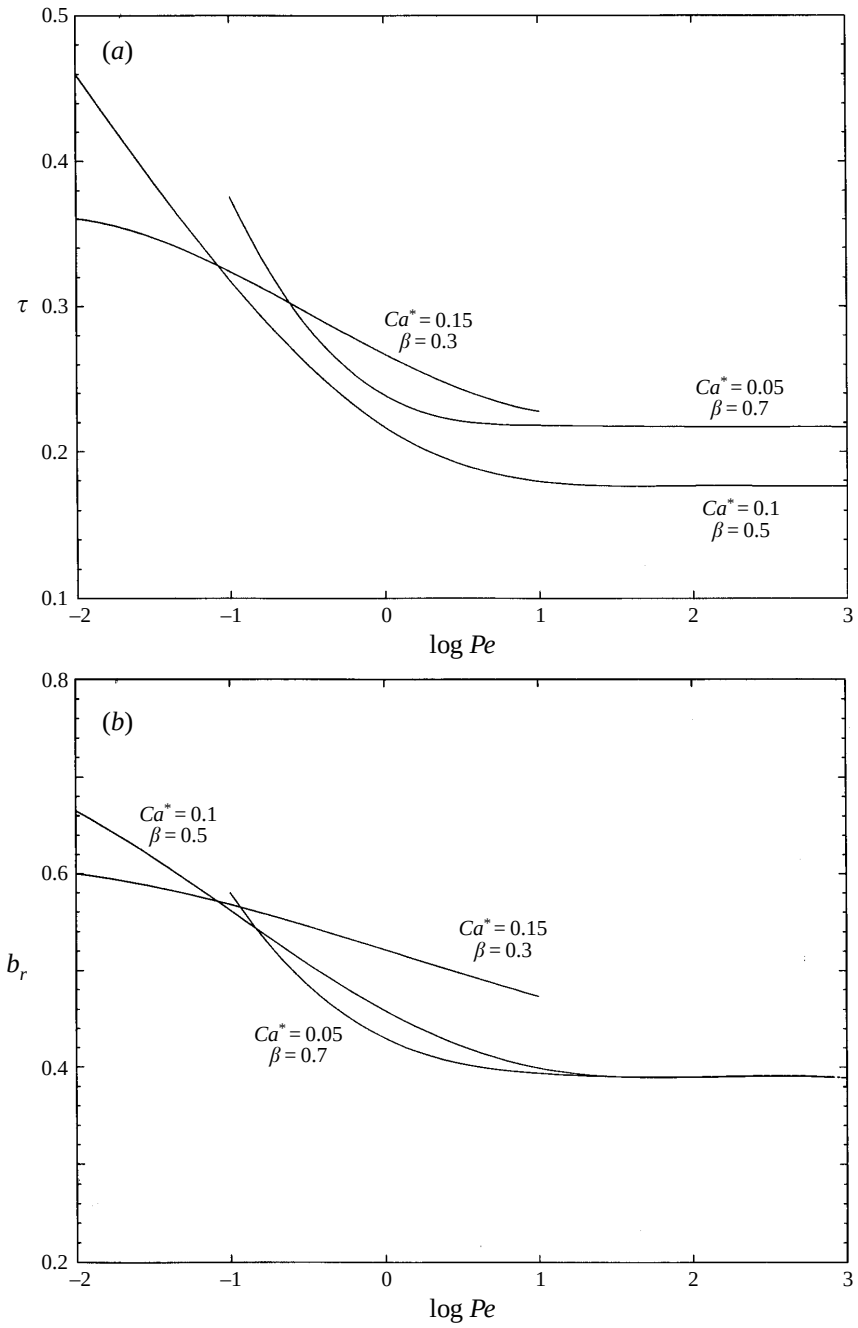

FIGURE 8. (*a*) Snap-off time and (*b*) radius of the bubble generated, as a function of Péclet number for $Ca^* = 0.05$, $\beta = 0.7$; $Ca^* = 0.1$, $\beta = 0.5$; and $Ca^* = 0.15$, $\beta = 0.3$.

interface become very small, which, in turn, requires increased curvature to satisfy the normal stress balance.

The pressure jump across the capillary tube gives important information on the behavior of a bubble through a constriction. In particular it can be measured experimentally. In figure 9, we plot the pressure jump for the three Péclet numbers

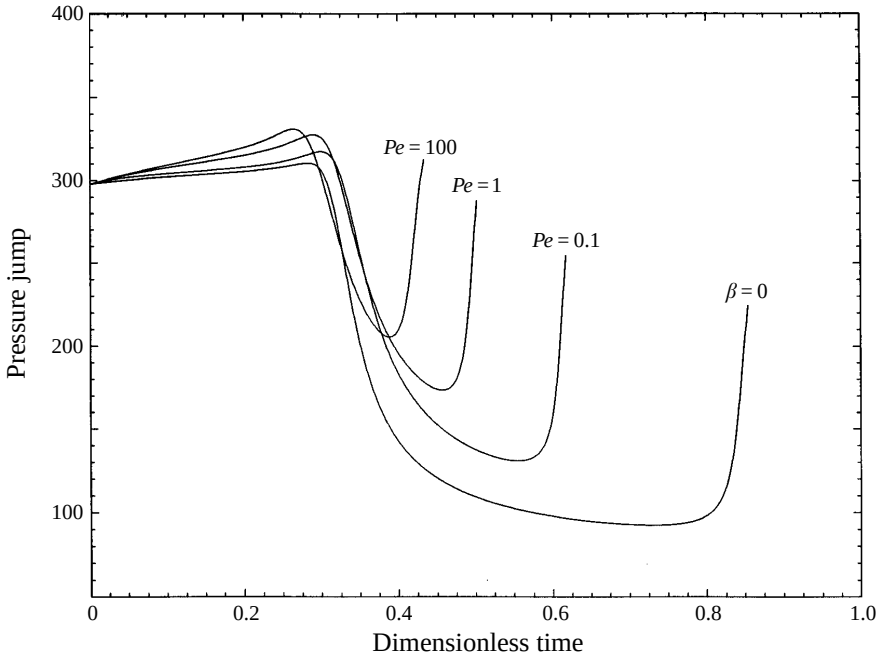

FIGURE 9. Pressure jump across the constricted capillary tube from $z = -6$ to $z = 6$ as a function of time for $Ca^* = 0.1$, $\beta = 0.5$, and $Pe = 0.1, 1, 100$; and $Ca^* = 0.1, \beta = 0$.

considered in figures 5 to 7, together with the pressure jump for the case of $\beta = 0$, as a function of time t. Here we define the pressure jump as the difference between the upstream and downstream pressure. Since the computational domain is finite, we have taken this to be the change in the pressure from $z = -6$ to $z = 6$. As shown in figure 9, the pressure jump increases as the front of the bubble enters the converging section of the constriction, it then decreases sharply as the bubble expands out of the constriction and reaches a minimum value just before bubble snap-off occurs. Finally, the pressure jump rises abruptly as the bubble is snapping off. This behaviour of the pressure jump across the constricted capillary tube is typical for the other values of the dimensionless parameter studied.

We now consider the effects of varying β while keeping the Péclet number and Ca^* fixed. In order to discuss the effects of varying β, it is important to remember that the physiochemical parameter β is a measure of sensitivity of the interfacial tension to the surfactant concentration. For a fixed surfactant distribution, increasing the value of β also increases the interfacial tension gradient. In figure 10 we plot the snap-off time and the effective radius b_r as a function of β for $Ca^* = 0.1$ and $Pe = 0.1, 1,$ and 100. We see that in general, τ and b_r decrease with β. In figures 11 and 12, we show the bubble evolution up to the occurrence of snap-off, the corresponding surfactant concentration on the bubble surface and the tangential surface velocity for $Ca^* = 0.1$, $Pe = 1$, and $\beta = 0.1, 0.7$, respectively (the case $\beta = 0.5$ is shown in figure 6). We find that the surfactant concentration shows increased variations as the value of β decreases. It should be noted that although the parameter Ca^* is held fixed in these figures, it is also implicitly dependent on β and requires that Ca decrease with increasing β.

As pointed out by Borhan & Mao (1992), the effects of β on the interfacial tension

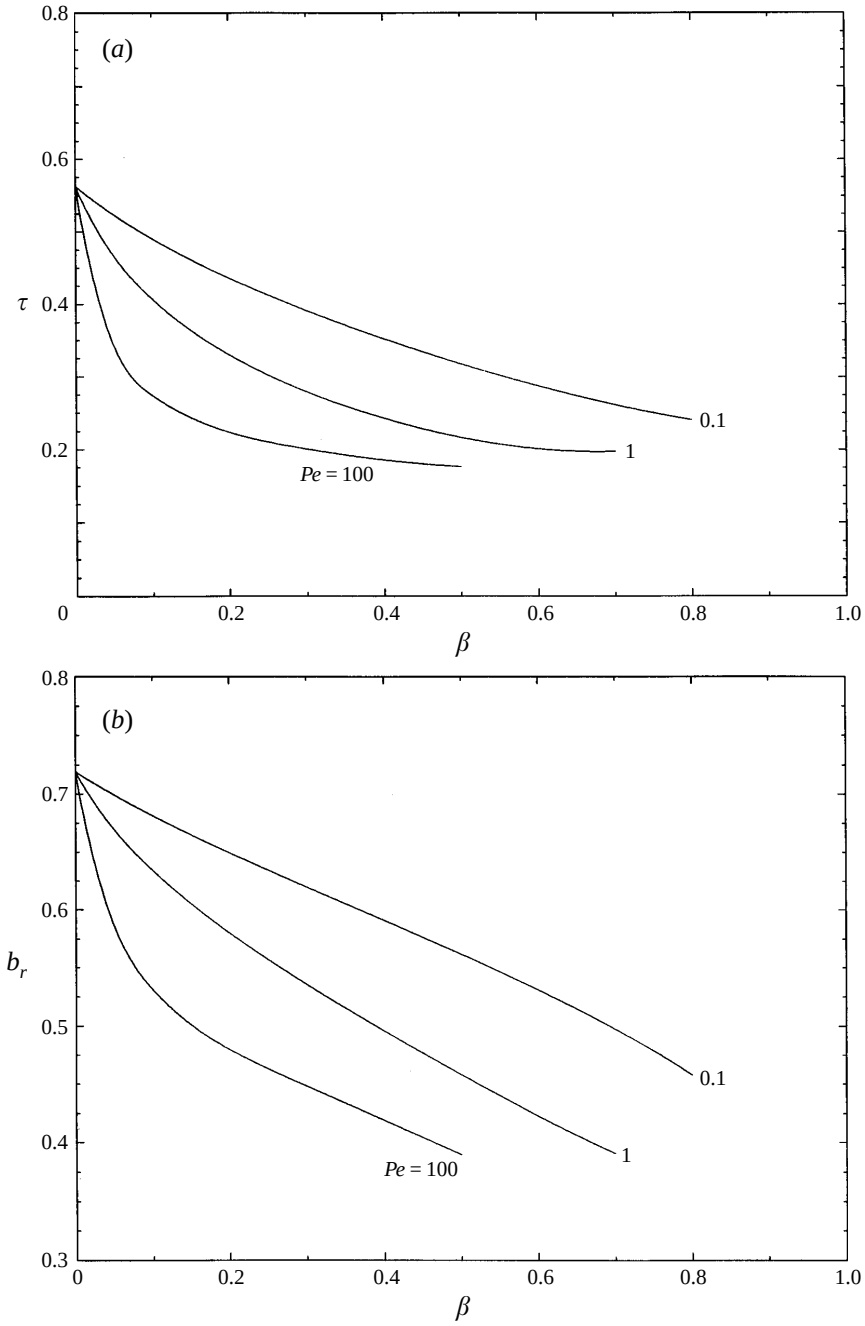

FIGURE 10. (*a*) Snap-off time and (*b*) the radius of the bubble generated, as a function of β for $Ca^* = 0.1$ and $Pe = 0.1, 1, 100$.

forces are actually given by the normalized interfacial tension $(1-\beta C)/(1-\beta)$, which is the ratio of the interfacial tension forces to the initial uniform interfacial tension forces on the bubble surface. The corresponding normalized interfacial tension forces for the bubbles shown in figures 11, 12, and 6 are plotted in figures 13(*a*) to 13(*c*). It is clear from these figures that although the variations in the surfactant concentration

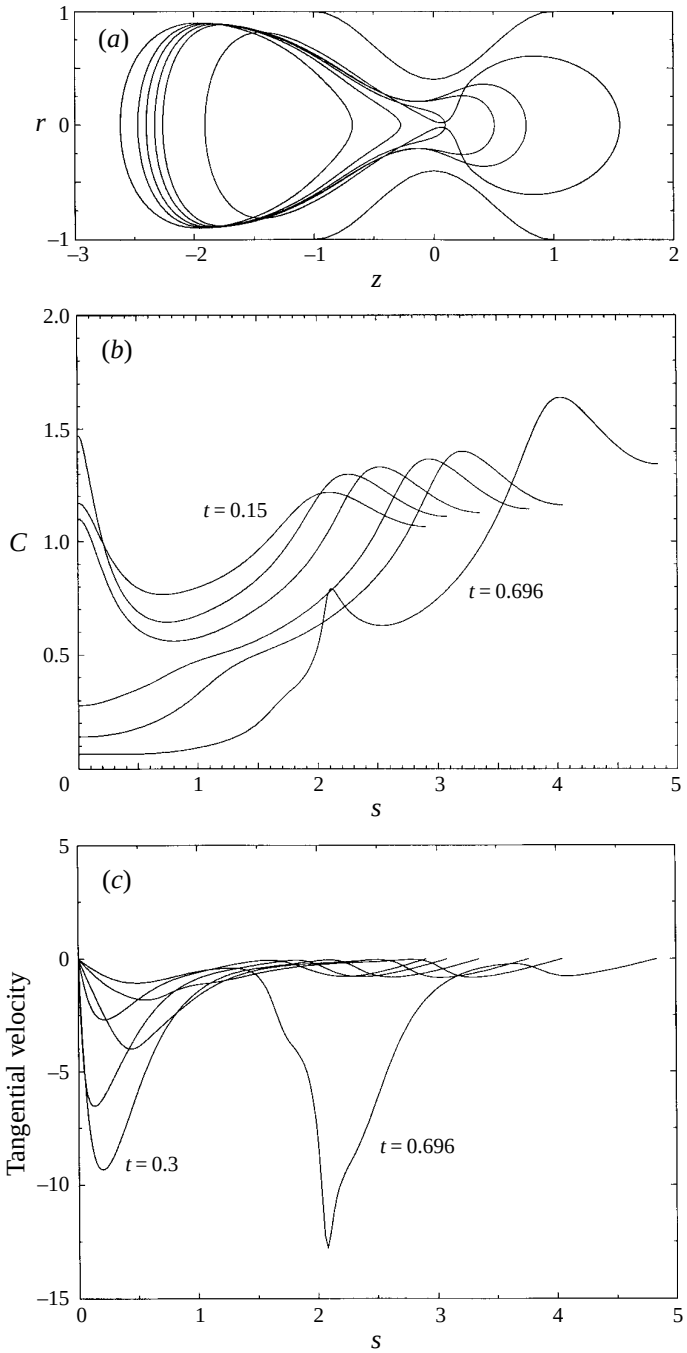

FIGURE 11. (*a*) Evolution of an initially spherical bubble with uniform surfactant concentration, (*b*) surfactant concentration and (*c*) surface velocity, for $Ca^* = 0.1$, $Pe = 1$, and $\beta = 0.1$, at times 0.15, 0.25, 0.3, 0.35, 0.4, and 0.696.

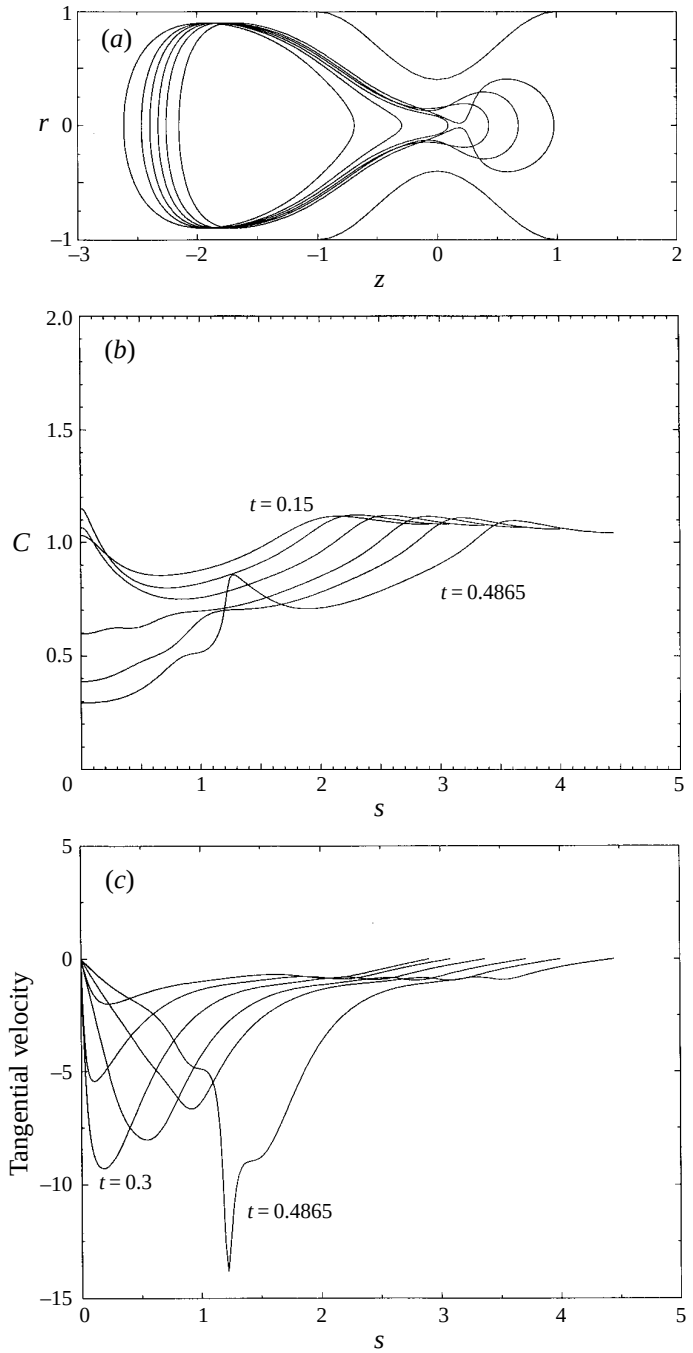

FIGURE 12. (*a*) Evolution of an initially spherical bubble with uniform surfactant concentration, (*b*) surfactant concentration and (*c*) surface velocity, for $Ca^* = 0.1$, $Pe = 1$, and $\beta = 0.7$, at times 0.15, 0.25, 0.3, 0.35, 0.4, and 0.4865.

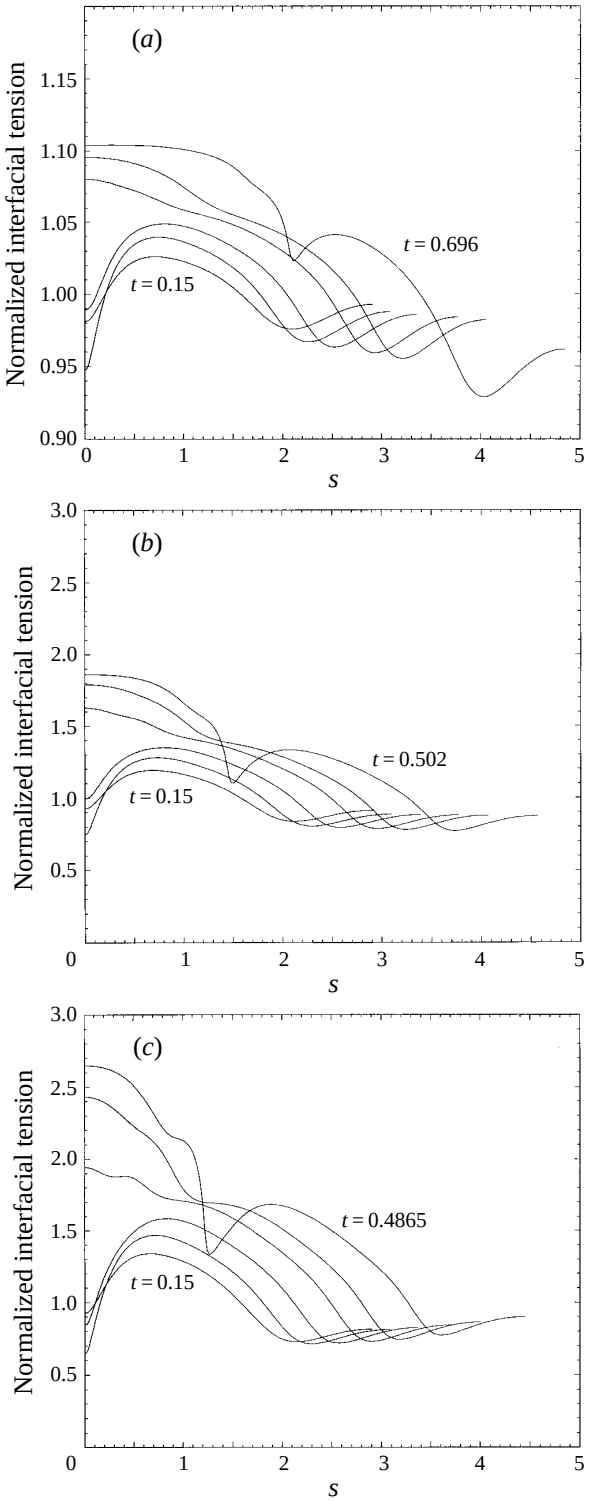

FIGURE 13. Normalized interfacial tension forces $\gamma/\gamma_s(1-\beta C)$ for $Ca^* = 0.1$, $Pe = 1$, (*a*) $\beta = 0.1$, at times 0.15, 0.25, 0.3, 0.35, 0.4, and 0.696; (*b*) $\beta = 0.5$, at times 0.15, 0.25, 0.3, 0.35, 0.4, and 0.502; and (*c*) $\beta = 0.7$, at times 0.15, 0.25, 0.3, 0.35, 0.4, and 0.4865.

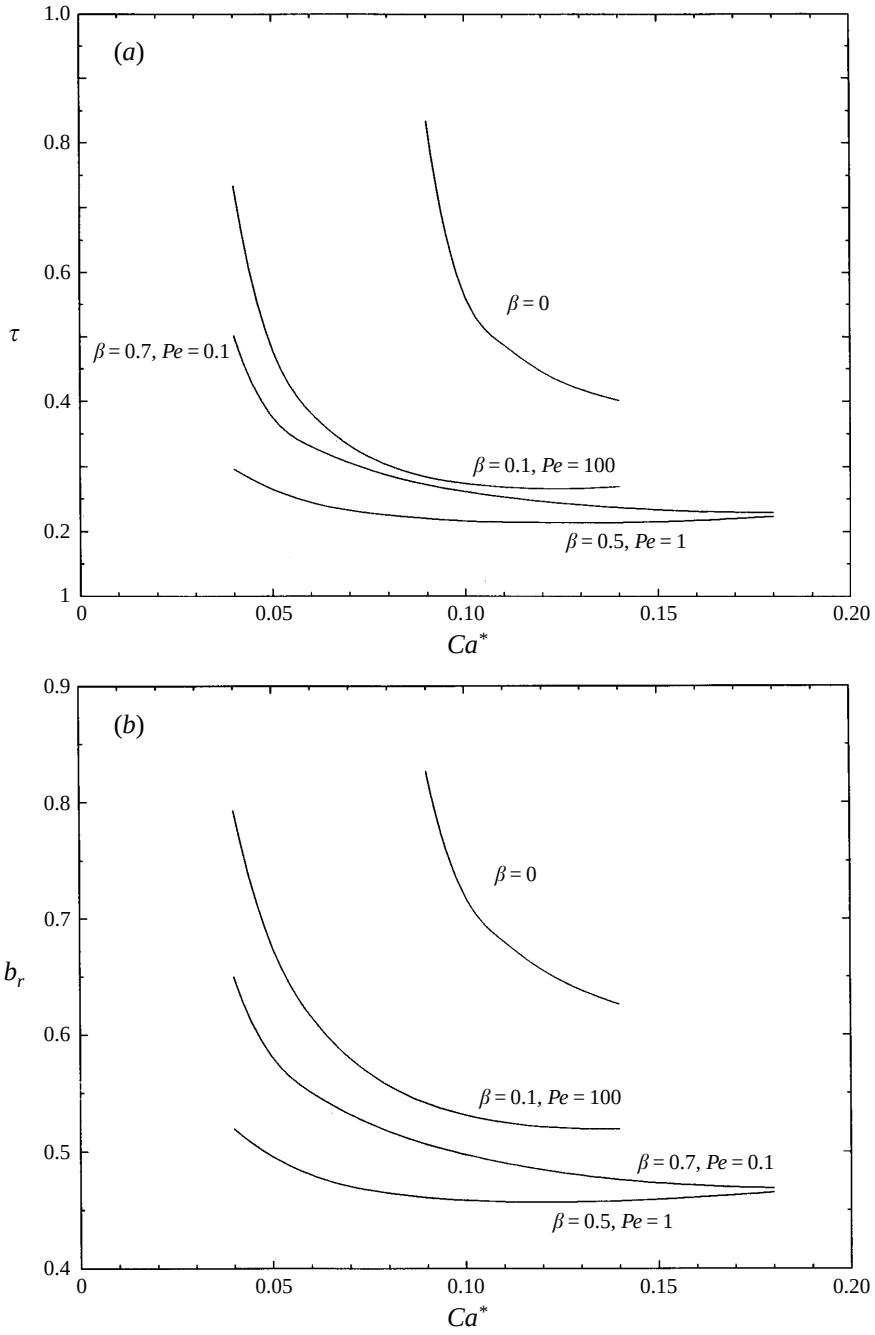

FIGURE 14. (*a*) Snap-off time and (*b*) the radius of the bubble generated, as a function of Ca^* for $\beta = 0.1$ and $Pe = 100$; $\beta = 0.5$ and $Pe = 1$; $\beta = 0.7$ and $Pe = 0.1$; and uniform surfactant concentration $\beta = 0$.

increase as the value of β decreases, the corresponding variations in the normalized interfacial tension forces on the bubble surface actually increase with increasing β. Consequently, larger interfacial tension gradients exist for larger values of β as the front of the bubble reaches the diverging section of the constriction and starts

expanding. This leads to the acceleration of the snap-off process for larger values of β. These computations were very sensitive to the number of grid points used and very time consuming. Hence because of the possible large numerical errors, our results for large β (beyond what is plotted) are inconclusive.

The effects of varying Ca^* on the snap-off time and the radius of the bubble generated are shown in figure 14 for different values of Pe and β. The case when surfactant concentration remains uniformly distributed throughout the motion ($\beta = 0$) is also included in these figures. From figure 14, we can see that the snap-off time and the effective radius of the bubble generated decrease when surfactant is present. We also see that the range of Ca^* for which bubble snap-off is found increases when surfactant is present. For the case of $\beta = 0$, bubble snap-off is observed when $0.09 \leqslant Ca^* \leqslant 0.14$. When surfactant transport takes place on the bubble surface, snap-off is observed when $0.04 \leqslant Ca^* \leqslant 0.14$ for $\beta = 0.1$ and $Pe = 100$. This range increases to $0.04 \leqslant Ca^* \leqslant 0.18$ for $\beta = 0.5$, $Pe = 1$ and for $\beta = 0.7, Pe = 0.1$. For a fixed value of β and Péclet number, increasing the value of Ca^* implies that the viscous forces become important. This leads to increased deformations due to the increased shearing forces on the bubble surface and hence decreases the snap-off time and the effective radius b_r. This observation is consistent with the case of constant surface tension ($\beta = 0$) studied in TM. In figures 15 and 16, we show the bubble evolution, the corresponding surfactant concentration on the bubble surface and the tangential surface velocity for Ca^* equal to 0.04 and 0.18 ($\beta = 0.5$ and $Pe = 1$). The case where $Ca^* = 0.1, \beta = 0.5$, and $Pe = 1$ is shown in figure 6. We note that in general, for the cases shown in figure 14, snap-off time and the effective radius appear to be decreasing functions of Ca^* although for the larger-Pe cases we see a slight increase for the larger values of Ca^*. We also notice that in figure 16, the snap-off point is shifted further downstream compared to the cases of smaller Ca^*. Examining the surface velocity fields, we find that the magnitude of the normal velocity is similar for the cases when $Ca^* = 0.1$ and $Ca^* = 0.18$ before snap-off occurs. However, as the bubble is snapping off, the magnitude of the normal velocity for $Ca^* = 0.18$ is actually smaller than the $Ca^* = 0.1$ case; this delays the occurrence of the snap-off process and a larger bubble is generated.

5. Conclusions

The effects of surfactant on the dynamics of a liquid drop and gas bubble moving in a straight or constricted capillary tube have been investigated numerically. We find that if the normalized capillary number, Ca^*, is small enough, then steady-state solutions are possible in a straight capillary tube. A similar conclusion holds for small values of the parameter β. As either of these parameters increases, the drop develops a re-entrant cavity at its rear forming a winged shape profile. Surfactant is accumulated at the tips of these wings, which, in turn, increases $\partial^2 C/\partial s^2$, the curvature and the surface velocity gradients there. Our computations end when these variables become very large in magnitude. We find that the surfactant increases the rate at which the re-entrant cavity enters the drop, and this rate is found to increase with Péclet number for the cases we have studied. These computations imply several possibilities for large Ca^* or β. First a steady-state solution could still exist but the values of the velocity gradients and the other parameters are so large that we are not able to capture it well with our current numerical scheme. Second, as with the uniform-surfactant case, a re-entrant cavity may be moving into the drop but again the large values of the dependent variables limit our ability to tract the solution. Or

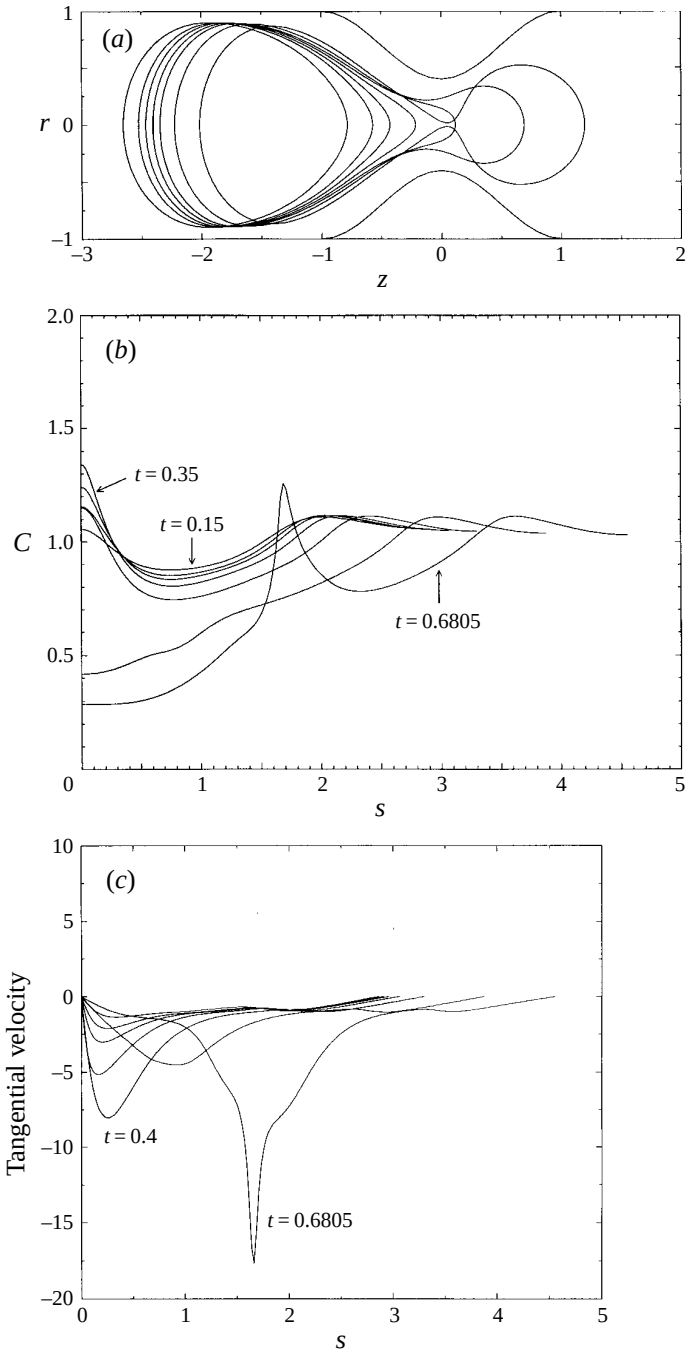

FIGURE 15. (*a*) Evolution of an initially spherical bubble with uniform surfactant concentration, (*b*) surfactant concentration and (*c*) surface velocity, for $Ca^* = 0.04$, $Pe = 1$, and $\beta = 0.5$, at times 0.15, 0.25, 0.3, 0.35, 0.4, 0.5, and 0.6805.

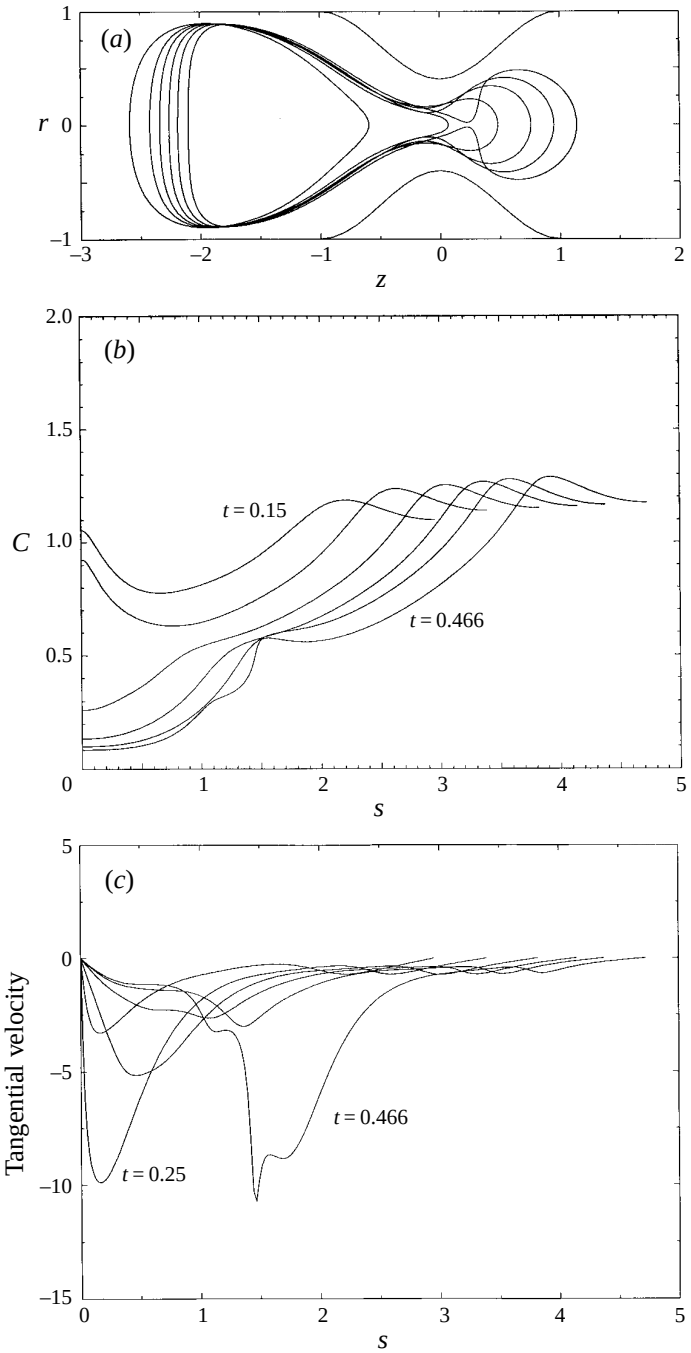

FIGURE 16. (*a*) Evolution of an initially spherical bubble with uniform surfactant concentration, (*b*) surfactant concentration and (*c*) surface velocity, for $Ca^* = 0.18$, $Pe = 1$, and $\beta = 0.5$, at times 0.15, 0.25, 0.3, 0.35, 0.4, and 0.466.

third, it may be possible that with surfactants, one of the dependent variables or its derivative becomes singular in finite time, which would require a reformulation of the problem after the singularity is formed. Along with this is the possibility that the surface tension tends to zero signalling the need for an improved equation of state. There are other equations of state more realistic than the linear model presented here, e.g. the Frumkin equation of state, but the linear model was chosen here since it is simple and should have features similar to other models. Additional work is necessary to precisely identify what is occurring in this straight tube drop motion problem. We note that in all of our calculations, axisymmetry is assumed and this may be violated in a real situation.

The effects of surfactant on the dynamics of a bubble in a constricted capillary tube have been the main focus of this study. This is a very complicated free boundary problem in which the bubble evolution is coupled to the distribution and evolution of surfactant along the surface. Hence the dynamics is strongly coupled to the initial bubble shape, location and surfactant distribution. Nevertheless, some trends have been identified in how the parameters effects the snap-off time. For example, we find that surfactant tends to decrease the snap-off time and decrease the size of the bubble being snapped-off. In a situation similar to the evolution into steady solutions in the straight tube, when snap-off is not observed, our computations end when the values of the derivatives of the dependent variables become large at the rear of the bubble. For the parameter ranges we have considered, the time scales for these two phenomena appear to be distinct, hence we feel confident of our predictions of snap-off time (e.g. figures 8, 10 or 14). Finally we note that our numerical simulations have given us a better understanding of the effects of the different parameters on the dynamical interplay between the surfactant distribution along the bubble surface and the bubble dynamics.

This research was supported in part by Department of Energy grant DE-FG02-88ER13927.

REFERENCES

Aris, R. 1962 *Vectors, Tensors, and the Basic Equations of Fluid Mechanics*. Prentice-Hall.

Borhan, A. & Mao, C. F. 1992 Effect of surfactants on the motion of drops through circular tubes. *Phys. Fluids* A **4**, 2628–2640.

Bretherton, F. P. 1961 The motion of long bubbles in tubes. *J. Fluid Mech.* **10**, 166–188.

Ginley, G. M. & Radke, C. J. 1989 The influence of soluble surfactants on the flow of the long bubbles through a cylindrical capillary. *ACS Symposium Series* vol. 396, pp. 480–501.

Grotberg, J. B. 1994 Pulmonary flow and transport phenomena. *Ann. Rev. Fluid Mech.* **26**, 529–571.

He, Z., Dagan, Z. & Maldarelli, C. 1991 The influence of surfactant adsorption on the motion of a fluid sphere in a tube. Part 1. Uniform retardation controlled by sorption kinetics. *J. Fluid Mech.* **222**, 1–32.

Leyrat-Maurin, A. & Barthes-Biesel, D 1994 Motion of a deformable capsule through a hyperbolic constriction. *J. Fluid Mech.* **279**, 135–163.

Martinez, M. J. & Udell, K. S. 1990 Axisymmetric creeping motion of drops through circular tubes. *J. Fluid Mech.* **210**, 565–591.

Milliken, W. J. & Leal, L. G. 1994 The influence of surfactant on the deformation and breakup of a viscous drop: The effect of surfactant solubility. *J. Colloid Interface Sci.* **166**, 275–285.

Milliken, W. J., Stone, H. A. & Leal, L. G. 1993 The effect of surfactant on the transient motion of Newtonian drops. *Phys. Fluids* A **5**, 69–79.

Olbricht, W. L. 1996 Pore-scale prototypes of multiphase flow in porous media. *Ann. Rev. Fluid Mech.* **28**, 187–213.

Olbricht, W. L. & Kung, D. M. 1992 The deformation and breakup of liquid drops in low Reynolds number flow through a capillary. *Phys. Fluids* A **4**, 1347–1354.

Park, C. W. 1992 Influence of soluble surfactants on the motion of a finite bubble in a capillary tube. *Phys. Fluids* A **4**, 2335–2347.

Pozrikidis, C. 1991 *Boundary Integral and Singularity Methods for Linearized Viscous Flow*. Cambridge University Press.

Ratulowski, J. & Chang, H.-C. 1990 Marangoni effects of trace impurities on the motion of long gas bubbles in capillaries. *J. Fluid Mech.* **210**, 303–328.

Roof, J. G. 1970 Snap-off of oil droplets in water-wet pores. *Soc. Petrol Engrs J.* **10**, 85–90.

Stone, H. A. 1990 A simple derivation of the time-dependent convective-diffusion equation for surfactant transport along a deforming interface. *Phys. Fluids* A **2**, 111–112.

Stone, H. A. & Leal, L. G. 1990 The effects of surfactants on drop deformation and breakup. *J. Fluid Mech.* **220**, 161–186.

Tsai, T. M. 1994 Numerical solution of free boundary problems with surface tension at low Reynolds numbers. PhD Thesis, Department of Engineering Sciences and Applied Mathematics, Northwestern University.

Tsai, T. M. & Miksis, M. J. 1994 Dynamics of a drop in a constricted capillary tube. *J. Fluid Mech.* **274**, 197–217 (referred to herein as TM).

Wassmuth, F., Laidlaw, W. G. & Coombe, D. A. 1993 Calculation of interfacial flows and surfactant redistribution as a gas/liquid interface moves between two parallel plates. *Phys. Fluids* A **5**, 1533–1548.